Cellular Physiology and Biochemistry

Cell Physiol Biochem 2020;54:899-916
DOI: 10.33594/000000277
Published online: 19 September 2020
Accepted: 9 September 2020

Original Paper

Elucidation of the Mechanisms for the Underlying Depolarization and Reversibility by Photoactive Molecule

Tomohiro Numata[a] Ryosuke Fukuda[b] Mitsuru Hirano[c] Kazuma Yamaguchi[c,d] Kaori Sato-Numata[a,e] Hiroshi Imahori[f,g] Tatsuya Murakami[b,g]

[a]Department of Physiology, School of Medicine, Fukuoka University, Fukuoka, Japan, [b]Department of Biotechnology, Graduate School of Engineering, Toyama Prefectural University, Toyama, Japan, [c]Department of Synthetic Chemistry and Biological Chemistry, Graduate School of Engineering, Kyoto University, Kyoto, Japan, [d]Hiroshima Regional Taxation Bureau, Hiroshima, Japan, [e]Japan Society for the Promotion of Science, Tokyo, Japan, [f]Department of Molecular Engineering, Graduate School of Engineering, Kyoto University, Kyoto, Japan, [g]Institute for Integrated Cell-Material Sciences (iCeMS), Kyoto University Institute for Advanced Study (KUIAS), Kyoto University, Sakyo-ku, Kyoto, Japan

Key Words
Photo-induced depolarization • Membrane capacitance • Potassium channel • Patch-clamp • Photo-induced charge-separation molecule

Abstract
Background/Aims: Light-induced control of the cell membrane potential has enabled important advances in the study of biological processes involving the nervous system and muscle activity. The use of these light-induced modifications is expected in various medical applications, including the control of physiological responses and the recovery of lost functions by regulating nerve activity. In particular, charge-separating linkage molecules (Charge-Separation (CS) molecules) can depolarize cells by photoexcitation without genetic processing. However, the molecular mechanisms underlying cell membrane depolarization are unknown and have hindered its application. Here, we show that CS molecules localized in the cell membrane of PC12 cells using a high-density lipoprotein (HDL)-based drug carrier can excite the cells through a novel membrane current regulation mechanism by light irradiation. ***Methods:*** Membrane potential, channel activity, and membrane capacitance were measured by patch clamp method in rat adrenal gland pheochromocytoma (PC12) cells and K_V-overexpressing PC12 cells. CS molecules localized in the cell membrane of PC12 cells using HDL-based drug carrier. The localization of CS molecule was measured by a confocal microscopy. The mRNA expression was tested by RT-PCR. ***Results:*** Current clamp measurements revealed that the photo-activated CS molecule causes a sharp depolarization of about 15 mV. Furthermore, it was shown by voltage clamp measurement that this mechanism inactivates the voltage-dependent potassium current and simultaneously generates photo-activated CS molecule

Tomohiro Numata,
Hiroshi Imahori,
Tatsuya Murakami

Department of Physiology, School of Medicine, Fukuoka University, Nanakuma 7-45-1, Jonan-ku, Fukuoka-shi, Fukuoka, 814-0180 (Japan), E-Mail numata@fukuoka-u.ac.jp

Department of Molecular Engineering, Graduate School of Engineering, Kyoto University, Kyoto 615-8510 (Japan), E-Mail imahori@scl.kyoto-u.ac.jp

Department of Biotechnology, Graduate School of Engineering, Toyama Prefectural University, Toyama 939-0398 (Japan), E-Mail murakami@pu-toyama.ac.jp

induced (PACS) current owing to the loss of the cell membrane capacitance. This activity continues the depolarization of the target cell, but is reversible via a regenerative mechanism such as endocytosis and exocytosis because the cell membrane is intact. ***Conclusion:*** Thus, the mechanism of photo-induced depolarization concludes that photo-activated TC1 causes depolarization by generating PACS current in parallel with the suppression of the K^+ current. Moreover, the depolarization slowly restores by internalization of TC1 from the membrane and insertion of new lipids into the cell membrane, resulting in the restoration of K_V to normal activity and eliminating PACS currents, without cell damage. These results suggest the possibility of medical application that can safely control membrane excitation.

Introduction

Optogenetic therapies that enable local excitement have high potential as therapeutic strategies for neurological diseases, such as Alzheimer's, because they enable precise spatiotemporal control of cells [1]. Most of these technologies require prior gene manufacturing, such as the gene transfection of light-sensitive proteins or modification of target molecules with light-sensitive compounds, and their use is limited [2]. Using these applications adds technical complexity and risk. In contrast, quantum dots, gold nanomaterials, magneto-electric nanomaterials, piezoelectric nanomaterials, and caged compound have been shown to cause membrane excitation in cells simply by treating the cells with nanomaterials before stimulation [3-7]. Therefore, it is attractive as a tool for basic research and clinical applications related to various membrane excitations.

Despite increasing evidence that photosensitive compounds can be used to control cell function, the underlying mechanisms are inadequate. Photostimulation mediated by photosensitive compounds is thought to generate heat or reactive oxygen species, affect ion channel gene expression and gating, and excite cells by increasing membrane conductance [3, 8-10]. In part, this is because most previous experiments with light-induced charged molecules did not directly assay target cells through electrophysiology, but rather a downstream analysis of their effects (*e.g.*, imaging, biochemistry). Furthermore, studies on cells excited by light-induced molecular stimulation only change the state of the cells, and many studies still have the problem of reversibility and safety [11]. Thus, solving this problem will further advance research areas for cells and biological applications.

Here, the mechanism of photostimulation-induced depolarization by the photo-induced charge-separation (CS) molecular probe TC1, a ferrocene–zinc porphyrin–fullerene linked triad [12], in mammalian neural PC12 (rat pheochromocytoma) cells was directly investigated via electrophysiology. It was expected that the photoexcitation of TC1 would result in photo-induced electron transfer from the zinc porphyrin excited singlet state to the fullerene followed by a second electron transfer from the ferrocene to the zinc porphyrin radical cation, generating the ferrocenium cation-zinc porphyrin–fullerene radical anion pair in PC12 cell membrane [12]. We then attempted to perform membrane current measurements for an extended time, which showed that repolarization was possible by removing TC1 from the cell membrane via membrane transport. This finding has important implications for the photostimulation application of light-induced CS probes in the nervous system and other organs, and reports the effect of the cell membrane quality on membrane ion transport.

Materials and Methods

Cell culture and cDNA expression

Rat adrenal gland pheochromocytoma (PC12) cells and K_V-overexpressing PC12 cells were cultured in Dulbecco's modified Eagle's minimal essential medium (DMEM) with high glucose (Merck Millipore, Darmstadt, Germany) supplemented with 5% fetal bovine serum (FBS), 5% horse serum (HS), 30 U/mL penicillin and 30 μg/mL streptomycin (Nacalai Tesque, Inc., Kyoto, Japan) under 5% CO_2 and 95% air at 37°C.

PC12 cells were used for the following experiments with this culturing condition unless stated otherwise. PC12 cells for overexpression were plated on culture dishes for 24 hours. Then, the PC12 cells were transfected with K_V1.6-IRES2-AcGFP1, K_V2.1-IRES2-AcGFP1, K_V3.4-IRES2-AcGFP1, or K_V4.2-IRES2-AcGFP1. Lipofectamine 2000 (Invitrogen, Carlsbad, CA, USA) was used as the transfection reagent in accordance with the manufacturer's instructions. Electrophysiological measurements were performed at 36–72 h after transfection. Rat K_V1.6, K_V2.1, K_V3.4, and K_V4.2 (GenBank accession No. NM_023954, NM_013186, NM_001122776, and NM_031730.2, respectively) were cloned from rat whole brain Marathon-Ready cDNA (BD Biosciences, San Jose, CA, USA) using a PCR-based approach, and subcloned into the expression vector pIRES2-AcGFP1 (Clontech, Mountain View, CA, USA).

CS molecule and drug delivery system

Materials. The following materials were used as per the manufacturer's instructions. 1-Palmitoyl-2-oleoyl-glycero-3-phosphocholine (POPC: NOF Corporation, NY, USA), sodium cholate, dimethyl sulfoxide, (16:0) Liss Rhod PE (Avanti Polar Lipids), urea (Nacalai Tesque, Inc.), Spectra/Por Dialysis Membrane (Spectrum Laboratories, Inc., CA, USA), potassium bromide, Phospholipid C-test (FUJIFILM Wako Pure Chemical Corporation, Osaka, Japan), EMD Millipore Amicon Ultra-15 Centrifugal Filter Units (Fisher Scientific, MA, USA), DC Protein Assay Kit (Bio-Rad Laboratories, CA, USA), PD-10 desalting column (GE Healthcare, CA, USA). The donor–acceptor (D-A) linked molecule, TC1 was prepared according to the literature [12]. The TC1 molecule was designed to reduce the aggregation by increasing the bulkiness around the porphyrin moiety of the ferrocene–zinc porphyrin–fullerene (Fc–ZnP–C_{60}) triad [13]. The photo-induced charge-separation (CS) yields of TC1 are reported to be 50% in DMSO/H_2O mixture (1/99, v/v) and 18% in liposome in DMSO/H_2O (1/99, v/v) [12].

Preparation of genetically engineered HDL and loading of TC1 in HDL. The HDL mutant used in this study was prepared in accordance with a method reported previously with a minor modification [14]. The required amount of POPC and (16:0) Liss Rhod PE at a molar ratio of 99:1 was solubilized in phosphate buffered saline (PBS) containing 30 mg/mL sodium cholate (SC) at a molar ratio of lipid: SC = 1:3.9. The protein component of the mutant, which was an apoA-I protein with the N-terminal 44 amino acids deleted and a TAT (transactivator of transcription) peptide fused at the C-terminus, was solubilized in PBS containing 4 M urea and mixed with the above lipid/SC mixture at a protein:lipid molar ratio of 1:300. The mixture was incubated overnight at 4°C and then dialyzed against PBS at 4°C with a Spectra/Por Dialysis Membrane (MWCO = 50 kDa). The dialyzed dispersion was centrifuged at 20,000 × *g* at 4°C for 30 min to remove any debris. The obtained HDL sample was purified by density gradient ultracentrifugation in accordance with the method by Suda *et al.* [15] with minor modifications. Briefly, the density of the HDL sample (3 mL) was adjusted to 1.31 g/mL using potassium bromide. A four-step gradient solution of potassium bromide (9.0 mL, 1.21 g/mL; 11.4 mL, 1.063 g/mL; 9.9 mL, 1.019 g/mL; 3.6 mL, 1.006 g/mL) was prepared in a polyallomer tube (Beckman Coulter, Inc., Tokyo, Japan). Ultracentrifugation was carried out at 16°C in a HITACHI CP80NX using a 70 Ti rotor (Beckman Coulter, Inc.) at 286,000 × *g*. The sample was collected from a fraction in the 1.019 g/mL density range and was dialyzed against PBS at 4°C overnight. The dialysate was centrifuged at 20,000 × *g* at 4°C for 15 min. The supernatant was collected and concentrated with an Amicon Ultra Centrifugal Device (MWCO = 50 kDa) by centrifugation at 5,000 × *g* at 4°C until the total sample volume was ~3 mL. Incorporation of TC1 was conducted by following our previous methods [13]. Briefly, the HDL mutant (91 μg protein/mL) in PBS was mixed with TC1 in dimethyl sulfoxide (0.4 mM) at a volume ratio of 9:1, and then the mixture was incubated at room temperature for 1 h. The TC1-HDL mutant complex was purified with a PD-10 desalting column equilibrated with 0.9% NaCl.

Characterization of TC1-HDL mutant complex. The protein and POPC concentrations in the HDL mutant were determined by the Lowry method using the DC Protein Assay Kit and a phospholipid-specific enzymatic assay using the Phospholipid C-test Wako (FUJIFILM Wako Pure Chemical Corporation), respectively. The concentration of the CS molecules or (16:0) Liss Rhod PE was determined spectroscopically with a V-630 spectrophotometer (JASCO Corporation, Tokyo, Japan, 300–700 nm) or a Fluoromax 4 spectrophotometer (HORIBA, Ltd., Kyoto, Japan, 575–640 nm). The size distribution and zeta potential measurements were performed with a Nanotrac UPA-EX250 particle size analyzer (MicrotracBEL Corp., Osaka, Japan) in PBS and a Zetasizer Nano Z (Malvern Panalytical, Malvern, UK) in 20 mM Tris·HCl (pH 7.4) containing 10% PBS, respectively.

Confocal microscopy

PC12 cells were adhered to a poly-L-lysine (PLL) coated cover glass. After 24 h, the medium was removed, and the cells were washed once with Tyrode solution ((in mM) 140 NaCl, 5 KCl, 2 $CaCl_2$, 1 $MgCl_2$, 10 HEPES, and 10 D-glucose (pH adjusted to 7.4 with NaOH, and osmolality adjusted to 300 mOsmol/kg H_2O with D-mannitol) and resuspended with Tyrode solution. Then, an aqueous solution of the (16:0) Liss Rhodamine PE-labeled TC1-cell-penetrating (cpHDL) was added to the cells to adjust the concentration to a final value of 0.5 μM based on the compound. The cells were incubated for 3 min and washed with Tyrode solution once and resuspended in Tyrode solution with or without inhibitors. The cells incubated at room temperature (22-25°C) for 0 and 60 min after 2-min illumination (525–550 nm, input power 2 mW cm^{-2}, *see in Patch Clamp Measurements*), the cells were fixed with 4% paraformaldehyde (Nacalai Tesque, Inc.), and then mounted in Fluoromount-G mounting medium (Southern Biotechnology, Birmingham, AL, USA). Fluorescence images were acquired with a confocal laser-scanning microscope (Zeiss LSM710, Carl Zeiss Microscopy GmbH, Jena, Germany), which was equipped with a 40× oil objective lens. Rhodamine signals were acquired and line analyses were made with ZEN software (Carl Zeiss). Eight lines were drawn from the center with a 40° angle. The rhodamine signal for each line was considered positive when both points where the line crossed the edge of the cell showed a signal intensity above the half-maximum intensity. The relative rhodamine signal per cell was defined as the ratio of the positive lines.

Patch Clamp Measurements

Whole-cell patch recordings for the current clamp and voltage clamp were recorded using a nystatin-perforated patch technique on PC12 cells at room temperature (22–25°C) with an Axopatch 200B (Molecular Devices, Axon Instruments, Sunnyvale, CA, USA) patch-clamp amplifier. The patch electrodes prepared from borosilicate glass capillaries had a resistance of 4-5 MΩ. For perforated whole-cell recordings, low access resistance measurements were achieved by creating a blunt-tip electrode on the pipette that increased the total surface area of the membrane piece drawn into the pipette [16]. In nystatin-perforated whole cell recordings, series resistance (<15 MΩ) was compensated (to 70–80%) to minimize voltage errors. In current clamp recordings, currents were clamped to zero by the fast current clamp mode of the Axopatch 200B. Current signals were filtered at 5 kHz with a four-pole Bessel filter and digitized at 20 kHz. pCLAMP software (version 10.5: Molecular Devices, Axon Instruments) was used for command pulse control, data acquisition, and analysis. For membrane capacitance recordings were measured using the established conventional patch-clamp voltage application method [17]. Briefly, the membrane test mode of Clampex software (Molecular Devices, Axon Instruments) was used to obtain the values calculated from the capacitance component. The nystatin perforated patch was measured according to procedures based on previous reports [18, 19]. Briefly, the pipette tip was dipped into a normal pipette solution for about 10 seconds, then backfilled with the solution containing nystatin. Then, within a few minutes, we achieved a high input seal resistance by setting up the electrode holder, approaching the cell, and forming a giga-seal on the cell. The nystatin solution was dissolved by placing 200 mg of nystatin in 1 ma of dimethylsulfoxide (DMSO: FUJIFILM Wako Pure Chemical Corporation), vortex for 1 min, and then sonication for 10 min. From this stock solution, 1 μL was added to 1 mL pipette solution, vortexed again for 1 min, and sonicated for 10 min. The final solution was filtered through a 0.20 μm filter (Millipore Corporation, Japan) to obtain a pipette solution. This solution was used within the day. For conventional and nystatin-perforated whole-cell recordings, the Na^+-based bath solution contained (in mM) 140 NaCl, 5 KCl, 2 $CaCl_2$, 1 $MgCl_2$, 10 HEPES, and 10 D-glucose (pH adjusted to 7.4 with NaOH, and osmolality adjusted to 320 mOsmol/kg H_2O with D-mannitol). The pipette solution contained (in mM) 55 K_2SO_4, 20 KCl, 5 $MgCl_2$, 0.2 EGTA, and 5 HEPES (pH adjusted to 7.4 with KOH, and osmolality adjusted to 300 mOsmol/kg H_2O with D-mannitol). An Ag-AgCl pellet-3M KCl-agar bridge was used for reference electrode. The hν-induced V_m in Fig. 1 was calculated using the following equation: hν-induced V_m (mV) = V_{Ctl}–$V_{h\nu}$, where V_{Ctl} and $V_{h\nu}$ are the membrane potential values observed before and by the end of the illumination. I_{after} is a stable value of I after 30 minutes from illumination. I_1 and I_2 show a whole-cell current at +100 mV, and at –100 mV, respectively. For Fig. 2, 3, 4, 5, and 6, ramp pulses were applied every 5 s from –100 mV to +100 mV from a holding potential of −60 mV at a speed of 4 mV/ms. For Fig 6b, the recovery of membrane potential (%) was calculated using the following equation: recovery of membrane potential (%) = $((V_{peak}-V_{after})/(V_{peak}-V_{before})) \times 100$, where V_{before}, V_{peak} are the peaks values before and after illumination of V_m, respectively. V_{after} is a stable value of V_m after 30 minutes from illumination.

The recovery of K^+ current (%) in Fig. 6d was calculated using the following equation: recovery of K^+ current (%) = $((I_{peak1}-|I_{peak2}|)-(I_{after1}-|I_{after2}|))/((I_{peak1}-|I_{peak2}|)-(I_{before1}-|I_{before2}|))) \times 100$, where I_{before}, I_{peak} are the peaks values before and after illumination of I, respectively. I_{after} is a stable value of I after 30 minutes from illumination. The recovery of PACS current (%) in Fig. 6e was calculated using the following equation: recovery of PACS current (%) = $(|I_{peak2}|-|I_{after2}|))/(|I_{peak2}|-|I_{before2}|) \times 100$, where I_{before}, I_{peak} are the peaks values before and after illumination of I, respectively. The light used in the experiment was from a mercury lamp house (C-HGFIE: Nikon, Tokyo, Japan) attached to an inverted microscope Ti (Nikon) that excited cells through an objective lens through TRITC and ND filters (Nikon). The wavelength and intensity of the excitation light were measured with a spectrophotometer C-7000 (SEKONIC, Tokyo, Japan) and confirmed to be 525 to 550 nm and 2 mW cm^{-2}, respectively.

RNA isolation and RT-PCR

Total cellular RNA was extracted from PC12 cells using ISOGENE (Nippon Gene, Tokyo, Japan) in accordance with the protocol supplied by the manufacturer. Five hundred nanograms of total RNA were reverse-transcribed into the first-strand cDNA by use of the RNA LA PCR kit (AMV) Ver1.1 (Takara, Shiga, Japan) at a final volume of 20 µL. Expression levels of K_V 1–12 mRNA in PC12 cells were determined by RT-PCR. Gene-specific primers used for PCR were designed with Primer3 software (http://bioinfo.ut.ee/primer3/) and NCBI BLAST (www.ncbi.nlm.nih.gov/blast/) to identify complementary sequences in the rat genome. The primers used for PCR amplification and the predicted lengths of the PCR products are summarized in Supplementary Table S1 (for all supplementary material see www.cellphysiolbiochem.com). PCR was conducted with a GeneAmp PCR system 9700 (Applied BioSystems, Foster City, CA, USA) using LA Taq polymerase with GC buffer (Takara) for 32 cycles under the following conditions: initial denaturation was 3 min at 95°C, then 30 sec at 95°C, followed by a 30-sec annealing step at 63°C and 60-sec elongation at 72°C, and a final elongation of 7 min at 72°C. Each RT-PCR experiment was independently repeated twice to test the amplification reproducibility. The specificity of the amplicons was checked by sequencing the PCR products to confirm that its sequence corresponded to the target gene.

Detection of photo-induced cell damage

Detection of membrane damage was performed using the Cytotoxicity LDH Assay Kit-WST (Dojindo Laboratories, Kumamoto, Japan) in accordance with the manufacturer's protocol. Nuclear cell viability analysis was performed by double staining using acridine orange (AO) and propidium iodide (PI) assays. For the AO/PI reagents, a Cell Viability Kit (Logos Biosystems, Korea) was added to each sample. Briefly, reagent-loaded cells were left at room temperature for 5 minutes in accordance with the manufacturer's protocol, and then the cell sample images were obtained from a Countess II-FL automated cell counter (Thermo Fisher Scientific, Waltham, MA, USA). AO-positive cells were counted as live cells, and PI-positive cells were counted as necrotic cells. In these assays, TC1-treated cells were light-stimulated with Tyrode's solution for 5 minutes and then stimulated for 1 hour at room temperature under the same conditions as in the electrophysiology experiments. Each assay was performed three times and the results were analyzed statistically.

Drugs

The K^+ channel blockers and their suppliers were: tetraethylammonium (TEA: Sigma, St. Louis, MO, USA), 4-Aminopyridine (4-AP: Sigma), and XE-991 (10,10-bis(4-pyridinylmethyl)-9(10*H*) -anthracenone dihydrochloride: alomone labs, Jerusalem, Israel). The cation and anion channel blockers and their suppliers were: SKF96365 (1{β-[3-(4-methoxyphenyl)propoxyl]-4-methoxyphenethyl}-1H-imidazole hydrochloride: Sigma) and DIDS (4,4'-diisothiocyanostilbene-2,2'-disulfonic acid: Sigma). The blockers in Fig. 6, 7 and their suppliers were: brefeldin A (BFA), genistein (GEN), and phenylarsine oxide (PAO) were purchased from TCI (Tokyo, Japan). The TEA and 4-AP were dissolved in the experimental solution before use. Concentrated stock solutions of SKF96365 (10 mM), DIDS (100 mM), XE-991 (10 mM), BFA (50 mM), GEN (200 mM), and PAO (5 mM) were prepared in DMSO and stored at −20°C until required. The final concentration of DMSO was always kept below 0.1%, a concentration that did not interfere with the measurements.

Statistical analyses

All data are expressed as means ± SEM. We accumulated the data for each condition from at least three independent experiments. We evaluated statistical significance with Student's t-test for comparisons

between two mean values. The data in Fig. 1e were compared using one-way analyses of variance (ANOVA), followed by Tukey's multiple comparisons test. In all cases, a value of $P < 0.05$ was considered significant.

Results

TC1 loaded in a lipoprotein-based drug carrier causes efficient light-induced depolarization by decreasing K^+ current and increasing PACS current

Using an appropriate drug delivery system, light-induced CS molecules that efficiently localized to cell membranes caused large membrane depolarization [13]. The TC1 molecule, one of a series of previously developed CS molecules, showed only a very small depolarization (~6.3 mV) in cellular applications because it did not perform the appropriate drug delivery system strategy [12]. This greatly delayed its technological development for biological applications. Achieving more efficient depolarizing systems is a prerequisite for the development of biological tools and medical applications. Therefore, we adopted a previously developed discoidal high-density lipoprotein (HDL)-based drug carrier [14] that could be efficiently localized to the cell membrane. A system for encapsulating TC1 was designed to evaluate the light-induced depolarization in PC12 cells using nystatin-perforated whole-cell recordings.

As shown in Fig. 1, the cells treated with the TC1 molecule incorporated in cell-penetrating high-density lipoprotein (TC1-cpHDL) caused depolarization gradually after light irradiation, and reached a stable depolarization of 16 mV within 5 minutes after stimulation. In contrast, TC1 cells without cpHDL reached a stable depolarization of 6 mV with 10 min after stimulation. Cells without TC1 or cpHDL did not show a significant change in the membrane potential upon light irradiation. These results indicate that we developed a more efficient depolarizing system of TC1 that was 159% larger and twice as fast when using cpHDL in comparison with TC1 without the drug delivery system. This increase in efficiency is consistent with the current (Fig 7a, control) and previous results [12, 13] using cpHDL, which is due to the uniform dis-

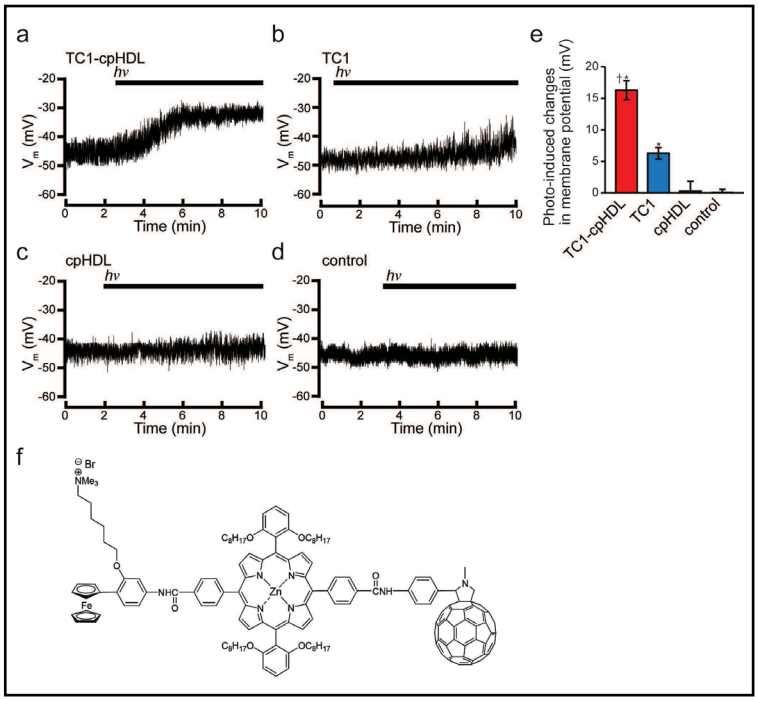

Fig. 1. Photo-induced depolarization of PC12 cells containing TC1. Representative traces of time-dependent changes in the membrane potential (V_m) under illumination (black bar, hν: 525–550 nm, input power 2 mW cm^{-2}) are shown for PC12 cells treated for 3 min with (a) TC1-loaded cell-penetrating high-density lipoprotein (TC1-cpHDL), (b) TC1, (c) cpHDL, (d) DMSO (control) and then washed with a Tyrode bath solution. (e) The average of the photo-induced changes in the membrane potential (mV) in TC1-cpHDL, TC1, cpHDL, and neither TC1 or cpHDL (control). (f) Molecular structure of TC1. TC1 is photo-induced charge-separation molecule consisting of ferrocene–zincporphyrin–fullerene (Fc–ZnP–C_{60}) triads (see Materials and Methods for details). *$p<0.05$ vs. control, †$p<0.05$ vs. TC1 ($n = 5$-7). hν: photon energy where h is Planck's constant 6.626×10^{-34}, ν is frequency.

tribution and increased number of CS molecules (i.e. from 1.6×10^6 to $2\text{-}3 \times 10^7$) inserted into the cell membrane. Also, TC1-cpHDL cells induced depolarization by illumination, and reached a specific range of depolarization, indicating that this recording was performed stably. Under the experimental conditions based on the above results, we then investigated the underlying membrane current that causes membrane potential changes.

Because rapid changes in the cell membrane potential often need to be driven by ion-flux, the effect of TC1 on the cell membrane currents in PC12 cells under nystatin-perforated patch clamps was next examined by voltage clamp. As shown in Fig. 2a and 2b, the current-voltage relationship induced by the ramp pulse in TC1-treated cells was found to show current properties with an outward rectification and a reversal potential of −75 to −80 mV (Fig. 2b, inset x). Next, photostimulation of the cells caused the whole-cell current to slowly increase at −100 mV, while simultaneously decreasing at 100 mV. Later, both changes reached a plateau within 5 minutes. (Fig. 2a–d). After the current reached the plateau, a reversal potential near 0 mV and a linear *I-V* curve was observed (Fig. 2b, inset y). Since the photostimulated CS molecule, TC1, generated a membrane current, we call this current the photoactivated CS molecule-induced (PACS) current.

The biophysical properties of the current shown in the cells before photostimulation are typical because they showed a value close to the ideal K^+ equilibrium potential, which was −82 mV from the experimental solution conditions. Furthermore, the channel activity increased with depolarization. These biophysical features suggested that this is a voltage-gated K^+ channel. A decrease in the outward current and a shift in the reversal potential to around 0 mV were observed after photostimulation, suggesting that the TC1 activity mainly suppressed the voltage-dependent K^+ currents.

To investigate the PACS current characteristics with a linear rectification increased by light stimulation, we tried to inhibit the ion channel activity by drugs. Photostimulation-induced whole-cell currents with linear *I-V* relationships were not affected by the application of sufficient amounts of 100 μM DIDS, a broad anion channel inhibitor [20], or 10 μM SKF96365 a broad cation channel inhibitor [21] (Fig. 3a–d).

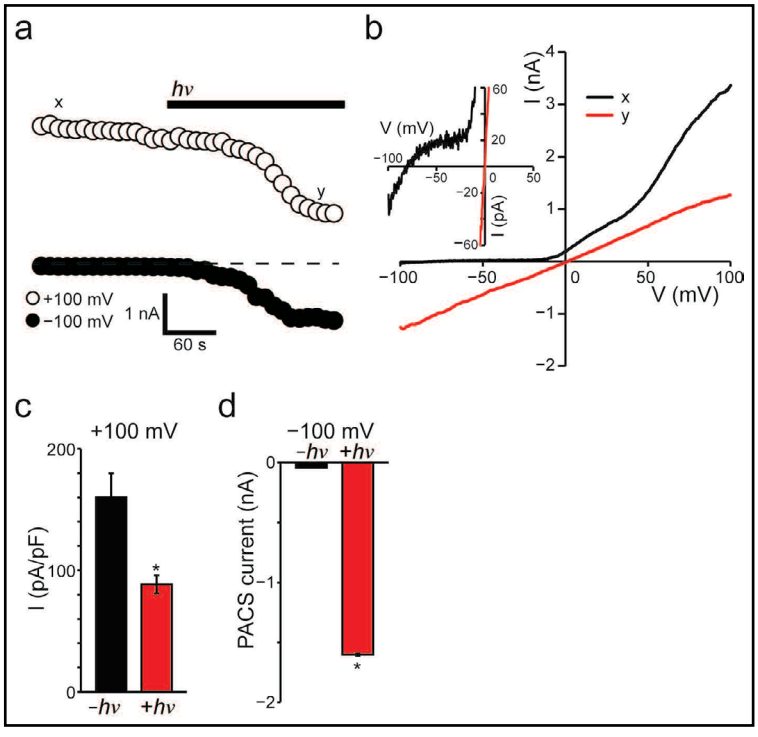

Fig. 2. Photo-induced change in the membrane current of PC12 cells containing TC1. Representative traces of time-dependent changes in the membrane current (a) and current–voltage (I–V) curve (b) under illumination (black bar, hν: 525–550 nm, input power 2 mW cm^{-2}) are shown for PC12 cells treated with TC1-loaded cpHDL. The dashed line indicates zero current level. The black and red curves in (b) were collected at the time points indicated by x and y, respectively, in (a). The insets in (b) show magnified views around the V-axis intercept. (c,d) The average of the photo-induced changes in the membrane current before (–hν) and after (+hν) illumination at +100 mV (c: current: I) and at −100 mV (d: photo-activated CS molecule induced (PACS) current), respectively. *p<0.05 vs. –hν (n = 5).

Electrophysiological membrane models generally assume that cell membranes are insulators and capacitors. However, because the membrane is not a perfect insulator, electricity may flow because the membrane capacity and permittivity are affected by physical changes such as the lipid content and the generation of conductive resistance. To examine the cell membrane properties, the membrane capacitance was measured using the established conventional patch clamp voltage application method [17]. As shown in Fig. 3e, photostimulation through TC1 gradually reduced the membrane capacitance. After an 8-minute stimulation time, the membrane capacitance was reduced by 24.7% in comparison with the control without TC1 (Fig. 3f). These results suggest that the photostimulated TC1 altered the membrane properties independently of ion transport, causing PACS currents.

TC1 suppresses intrinsic and extrinsic voltage-gated K^+ channels in PC12 cells

Because the data shown in Fig. 2 suggested that light-induced TC1 suppressed endogenously expressed voltage-gated K^+ (K_V) channels in PC12 cells, we investigated the molecular and functional basis of the K_V channels. PC12 cells are frequently used as a neuronal cell line, and the functional molecular expression of K_V1–3 has been previously reported [22]. However, no studies have comprehensively investigated K_V expression.

Robust amplification of PCR products of the expected size (see Supplementary Table S1) from the reverse transcribed RNA was obtained with specific primers for K_V1.1, K_V1.2, K_V1.3, K_V1.4, K_V1.5, K_V1.6, K_V2.1, K_V2.2, K_V3.1, K_V3.3, K_V3.4, K_V4.2, K_V4.3, K_V7.2, K_V7.3, K_V10.1, K_V11.1, K_V11.2, and K_V12.2. Sequencing analysis of K_V channels expressed endogenously in PC12 cells showed that almost all expressed K_V channel families were completely identical to the corresponding sequence of each rat voltage-gated K^+ channel (Fig. 4a).

Next, we attempted to perform pharmacological studies using the well-known K^+ channel blockers TEA and 4-AP, for the molecular classification of K_V channels and the K_V7-specific channel blocker XE-991. The voltage-gated K^+ channel current in the PC12 cells was inhibited by 50% with 5 mM TEA and 65% with 2 mM 4-AP. The current inhibition by XE-991

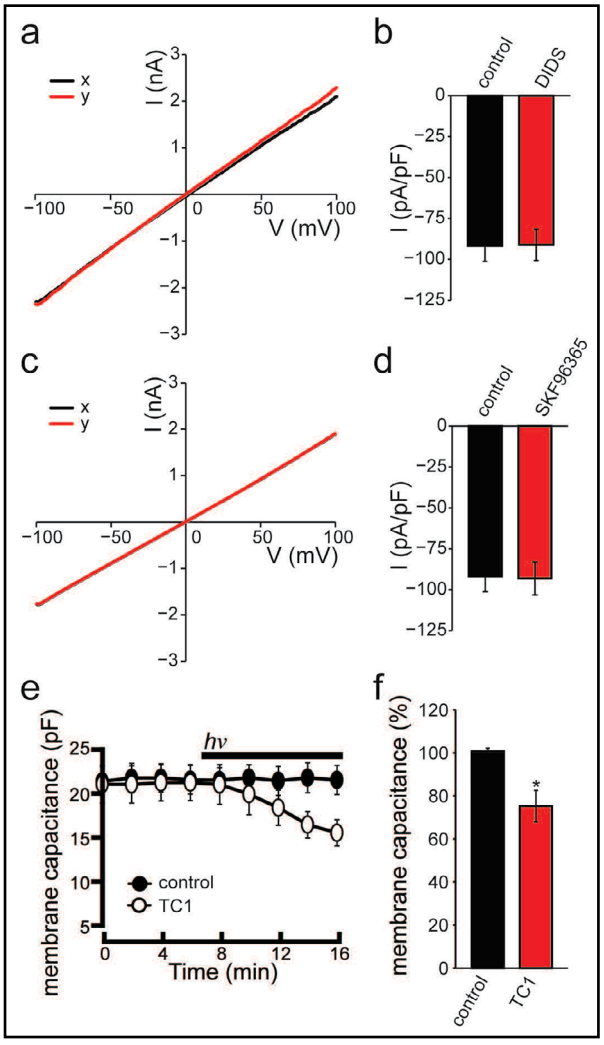

Fig. 3. Photo-induced changes in the membrane capacity of PC12 cells containing TC1. (a-d) Representative illumination-induced whole-cell currents (x: control), and effects of treatment with 100 µM DIDS (a: y, b: DIDS) and with 10 µM SKF96365 (c: y, d: SKF96365). (e) The time courses of the membrane capacitance in whole cell patch-clamp under illumination (black bar, hv: 525–550 nm, input power 2 mW cm^{-2}) are shown for PC12 cells treated in the presence of TC1-loaded cpHDL (TC1) and the absence of TC1 (control). (b) The average of the photo-induced changes in the membrane capacitance in the presence (TC1) and absence (control) of TC1. *p<0.05 vs. control (n = 5).

at 10 μM was minimal (<10%) and is summarized in Fig. 4b and 4c. K_V1, K_V4, and K_V7 were selected as candidates in consideration of the gene expression, the fact that the K^+ currents were activated near the resting membrane potential of PC12 cells (<0 mV, Fig. 4b, control), and because the molecular identification was based on low-potential (LVA)-type K_V channels. Furthermore, considering the pharmacological characterizations of TEA, 4-AP, and XE-991 [23, 24], K_V4 was found to be a current mainly suppressed by TC1. To investigate the TC1 target discrimination more clearly, an experimental PC12 cell system overexpressing rat $K_V4.2$, $K_V1.6$, $K_V2.1$, and $K_V3.4$ channels that showed relatively higher expression in *a* was constructed. As shown in Fig. 5a, almost all large outward currents observed with the control currents in $K_V1.6$, $K_V2.1$, $K_V3.4$ or $K_V4.2$ expressing cells were unexpectedly suppressed by photo-induced TC1 stimulation. All cells notably showed a PACS current of ~2 nA at −100 mV, similar to that seen in Fig. 2. Therefore, in the analysis of this experiment, the absolute value of the current obtained at −100 mV was subtracted from the current value obtained at +100 mV to obtain a purer K^+-derived current.

These results imply that TC1 suppresses all K_V channel types, thus making changes to the cell membrane that may commonly affect membrane transport proteins.

The TC1-induced depolarizing effect of light stimulation is reversible via membrane recycling

Previous work showed that photoreversibility studies on the effects of light-induced CS probes on cell-membrane depolarization remained a challenge [13]. In particular, the lack of CS molecule light-off reactions led to problems with the potential of safely using CS molecules for biological applications. To overcome these problems, we tracked the membrane

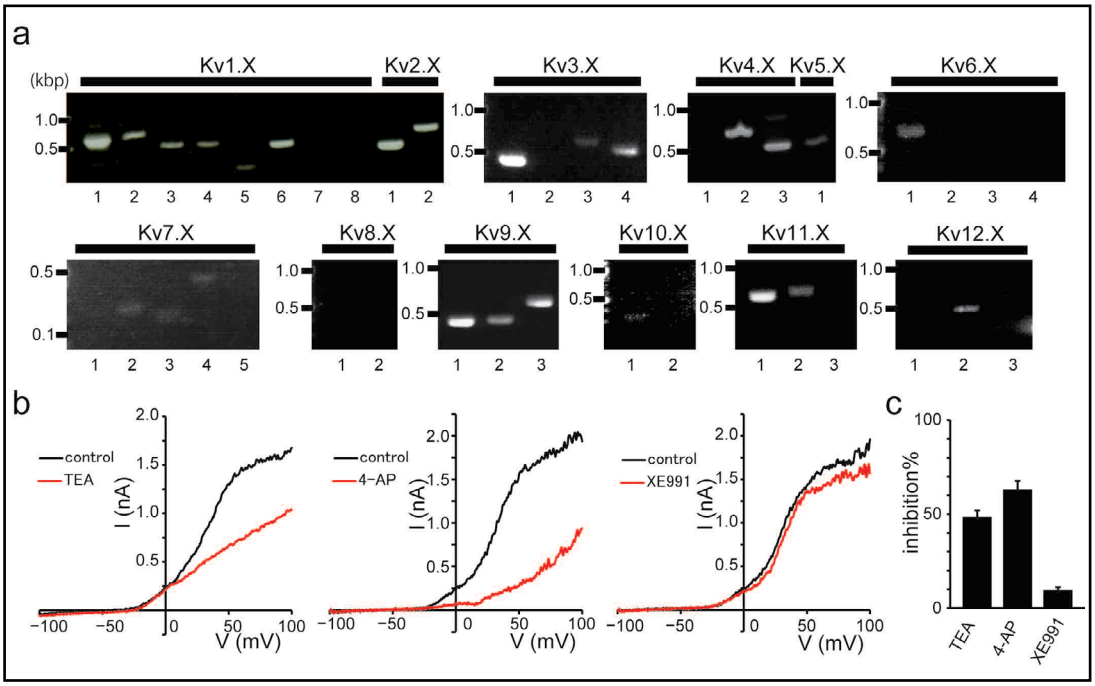

Fig. 4. Expression of mRNAs encoding K_Vs in PC12 cells. (a) The PC12 cells were used in RT-PCR for $K_V1.1$, 1.2, 1.3, 1.4, 1.5, 1.6, 1.7, 1.8, $K_V2.1$, 2.2, $K_V3.1$, 3.2, 3.3, 3.4, $K_V4.1$, 4.2, 4.3, $K_V5.1$, $K_V6.1$, 6.2, 6.3, 6.4, $K_V7.1$, 7.2, 7.3, 7.4, 7.5, $K_V8.1$, 8.2, $K_V9.1$, 9.2, 9.3, $K_V10.1$, 10.2, $K_V11.1$, 11.2, 11.3, and $K_V12.1$, 12.2, 12.3. Data are representative of triplicate experiments. (b) Pharmacological characterization of the endogenous K_V channel in membrane currents of PC12 cells. Effect of Tetraethylammonium (TEA), 4-Aminopyridine (4-AP), and XE-991. Representative recordings showing the effect of TEA (left column), 4-AP (center column), and XE-991 (right column) on endogenous K^+ currents. (c) The average of inhibition % of K^+ current (n = 5).

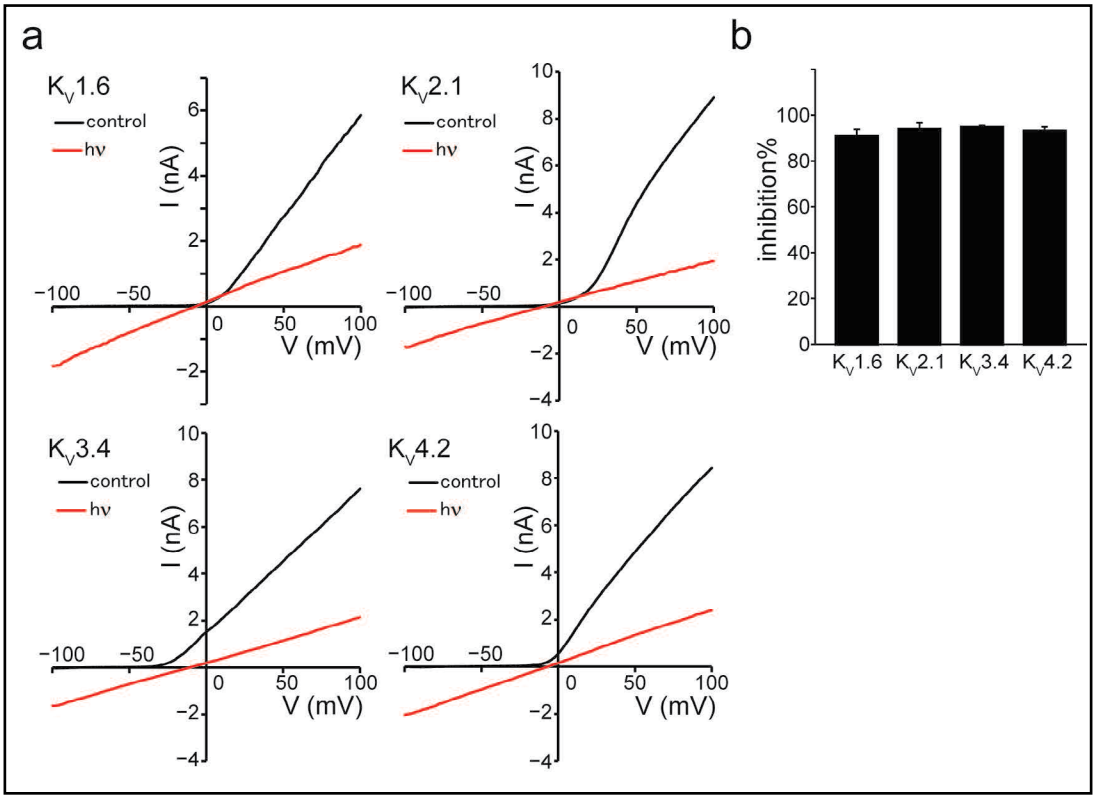

Fig. 5. Photo-induced change in the membrane current of K_V overexpressed in PC12 cells. (a) Representative I–V curves are shown for K_V1.6, K_V2.1, K_V3.4, or K_V4.2 expressing PC12 cells treated with TC1-loaded cpHDL before illumination (control) and after illumination (hν: 525–550 nm, input power 2 mW cm^{-2}). (b) The averages of the photo-induced percent inhibition in K_V current at +100 mV (n = 6–8).

potential and current through an incredibly long record of sustained depolarization, independent of the TC1 molecule off-response in PC12 cells.

As shown in the control of Fig. 6a, the light-induced TC1 activity caused a depolarization of approximately 15 mV (as in Fig. 1), followed by a sustained depolarization even after the irradiation was stopped. However, after 30–40 minutes of sustained depolarization, they surprisingly repolarized to the basal membrane potential (Fig. 6a, control). In addition, the membrane current underlying the membrane potential change was examined by evaluating the recovery rates of the K^+ current and PACS current to the initial recorded values (Fig. 6c–e, control).

One plausible mechanism of the cell membrane function recovery involves the recycling of membranes using endocytic and exocytotic pathways [25]. To further investigate this possibility, we examined the membrane potential and membrane current in the presence of inhibitors that target the membrane transport pathway.

Administration of brefeldin A (BFA), an inhibitor of the exocytosis pathway from the Golgi apparatus to the cell surface, had no effect on restoring the membrane potential in comparison with the controls (Fig. 6a and 6b: BFA). However, genistein (GEN), an inhibitor that blocks caveolae-mediated endocytosis, had a small effect on restoring the membrane potential. The clathrin-mediated endocytosis inhibitor phenylarsine oxide (PAO) also showed greater inhibition (Fig. 6a and 6b). As shown in Fig. 6c–e, the effect of membrane transport pathway inhibitors on the recovery of the K^+ current did not change with BFA treatment. However, the GEN and PAO treatments were significantly weakened. The effect of the PACS current on the recovery rate was reduced for all three treatments. The above results suggest that the endocytic pathway is important for the K^+ current restoration. Furthermore, both

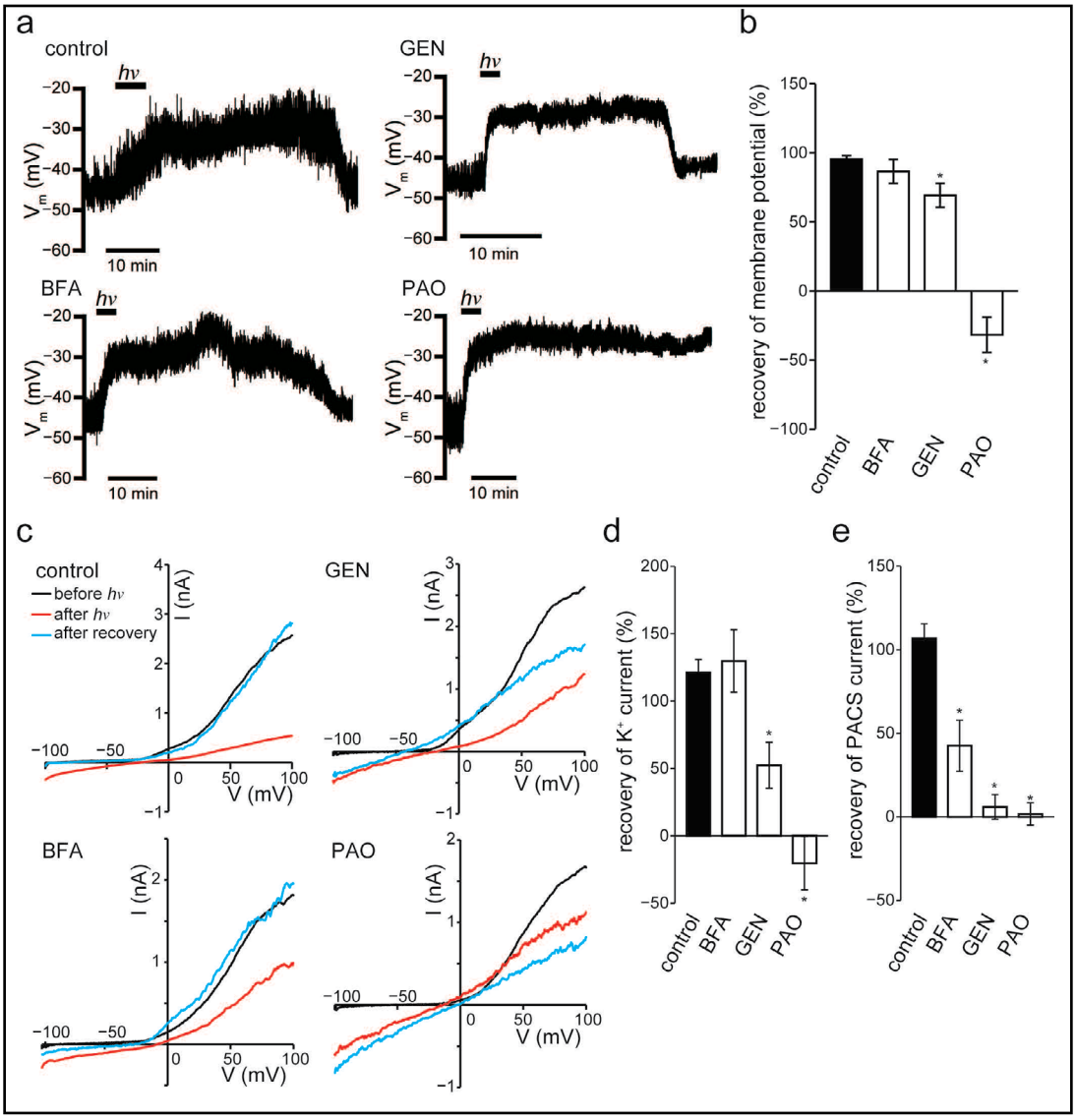

Fig. 6. Endocytic membrane retrieval involved in the recovery of photo-induced depolarization in PC12 cells. (a) Representative trace of time-dependent changes in the membrane potential under 4-min of illumination (black bar, hν: 525–550 nm, input power 2 mW cm^{-2}) are shown for PC12 cells treated with brefeldin A (BFA), genistein (GEN), and phenylarsine oxide (PAO). (b) The average of the membrane potential recovery. *p<0.05 vs. control (n = 5–7). (c) Representative I–V curves under 4-min of illumination (hν: 525–550 nm, input power 2 mW cm^{-2}) are shown for PC12 cells treated with TC1-loaded cpHDL. The black, red, and blue curves in (c) were collected at the time points before hν, after hν, and after recovery. (d) The average of the recovery of K^+ currents from photo-induced depolarization at +100 mV. *p<0.05 vs. control (n = 5–7). (e) The average of the recovery of PACS currents from photo-induced depolarization at –100 mV. *p<0.05 vs. control (n = 5–7).

exocytosis and endocytosis pathways are plausibly involved in the restoration of membrane lipids.

Finally, confocal microscopy was used to determine whether the membrane potential recovery upon depolarization from light-induced TC1 activity was dependent on changes in the TC1 localization. As shown in Fig. 7a, control, treatment of TC1-encapsulated rhodamine-labeled cpHDL was localized to the PC12 cell membrane at 0 minutes, which is consistent with a report that previously investigated the cell membrane localization of CS-encapsulated

cpHDL [13]. We then investigated the cellular localization of TC1 using the same membrane transport pathway inhibitors as with the experiment shown in Fig. 6. After 4 minutes of light stimulation on the TC1-treated cells, the rhodamine fluorescence observation disappeared 60 minutes later from the cell membrane in the control sample. The same was observed for the BFA-treated cells. However, the cells treated with GEN and PAO showed that the rhodamine fluorescence partially remained in the cell membrane. In a series of these experiments, LDH (lactate dehydrogenase) release experiments and PI/Hoechst staining showed that there was almost no damage to the cell membrane (Fig. 7c and 7d).

In summary, the TC1-induced depolarization from changes in the membrane property was repolarized before light stimulation by TC1 internalization and membrane function regeneration of intact PC12 cells via the membrane-trafficking system.

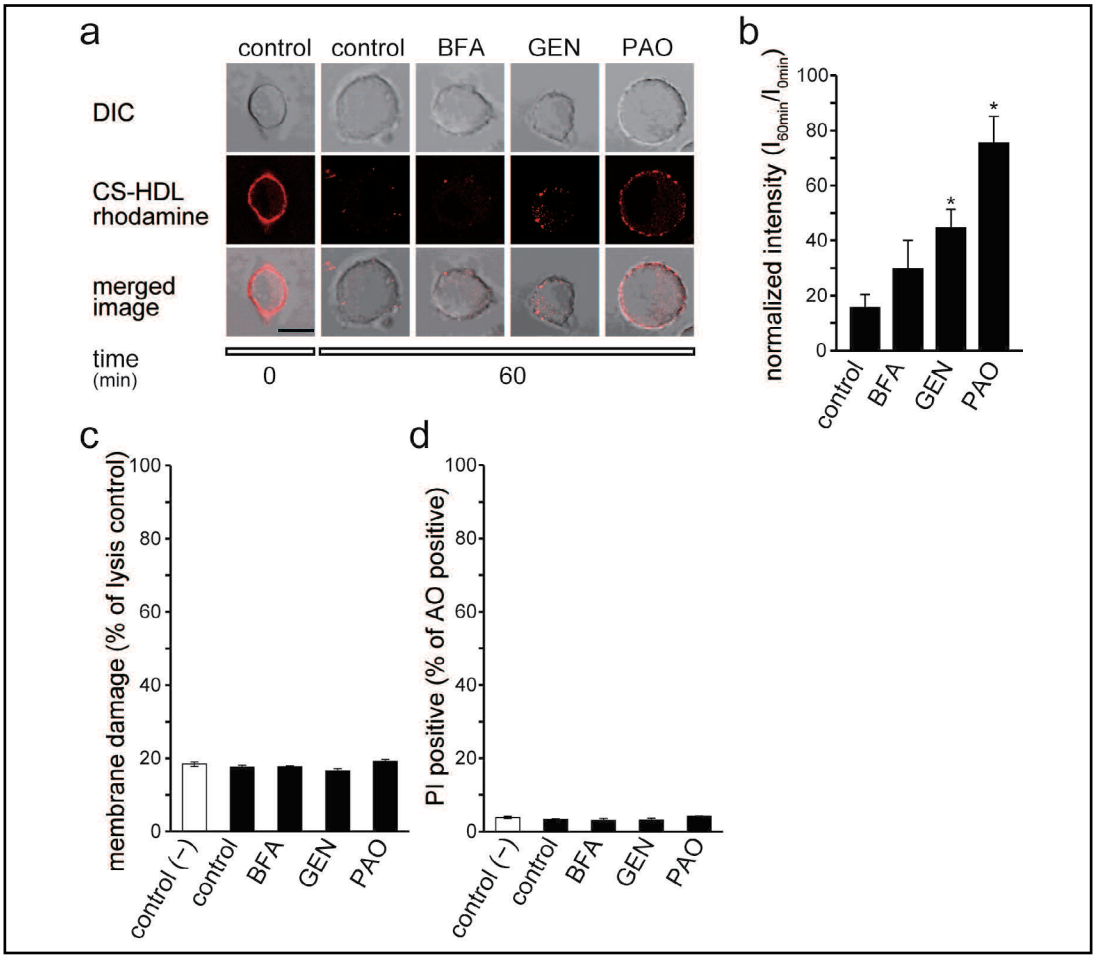

Fig. 7. Cell membrane localization of TC1-cpHDL at 60 min after photo-induced depolarization. (a) DIC (differential interference contrast) and confocal microscopy images of PC12 cells treated with TC1-cpHDL rhodamine (CS-HDL rhodamine), and treated with BFA, GEN, and PAO at 0 min (left panel) and 60 min. Filled bar indicates 10 μm. (b) The normalized intensities of rhodamine-positive lines of 10 total lines (see Materials and Methods) at 0 min and 60 min after 2-min illumination (hν: 525–550 nm, input power 2 mW cm^{-2}) are shown for PC12 cells treated with BFA, GEN, and PAO. *$p<0.05$ vs. control ($n = 5$). (c) Lactate dehydrogenase (LDH) assay for PC12 cells without TC1-cpHDL (control) and with TC1-cpHDL (black bar) treated with BFA, GEN, and PAO at 60 min after 2-min illumination (525–550 nm, input power 2 mW cm^{-2}). (d) Acridine Orange/Propidium Iodide (AO/PI) assay in PC12 cells without TC1-cpHDL (white bar) and with TC1-cpHDL (black bar) treated with BFA, GEN, and PAO at 60 min after 2-min illumination (525–550 nm, input power 2 mW cm^{-2}).

Discussion

Although the potential utility of photosensitive molecules, including photo-induced CS probes, has been demonstrated in recent cell biology studies, a poor understanding of the underlying mechanisms has slowed the development of valuable scientific and clinical applications. This study revealed an important and unexpected mechanism that causes the light-induced depolarization of CS molecules. This reversibility from depolarization has been shown to cause repolarization in correlation with cell membrane recycling (Fig. 8).

Controlling the membrane potential by photochemical switching is well known as an attractive way to control cellular and biological functions, as demonstrated in optogenetics and caged compounds. In particular, the control of membrane excitability using a photosensitive compound does not involve genetic manipulation, and may lead to attractive applications for disease treatment through realistic neural activity control. However, the control of a light-induced membrane potential, using photosensitive compounds, has not been fully elu-

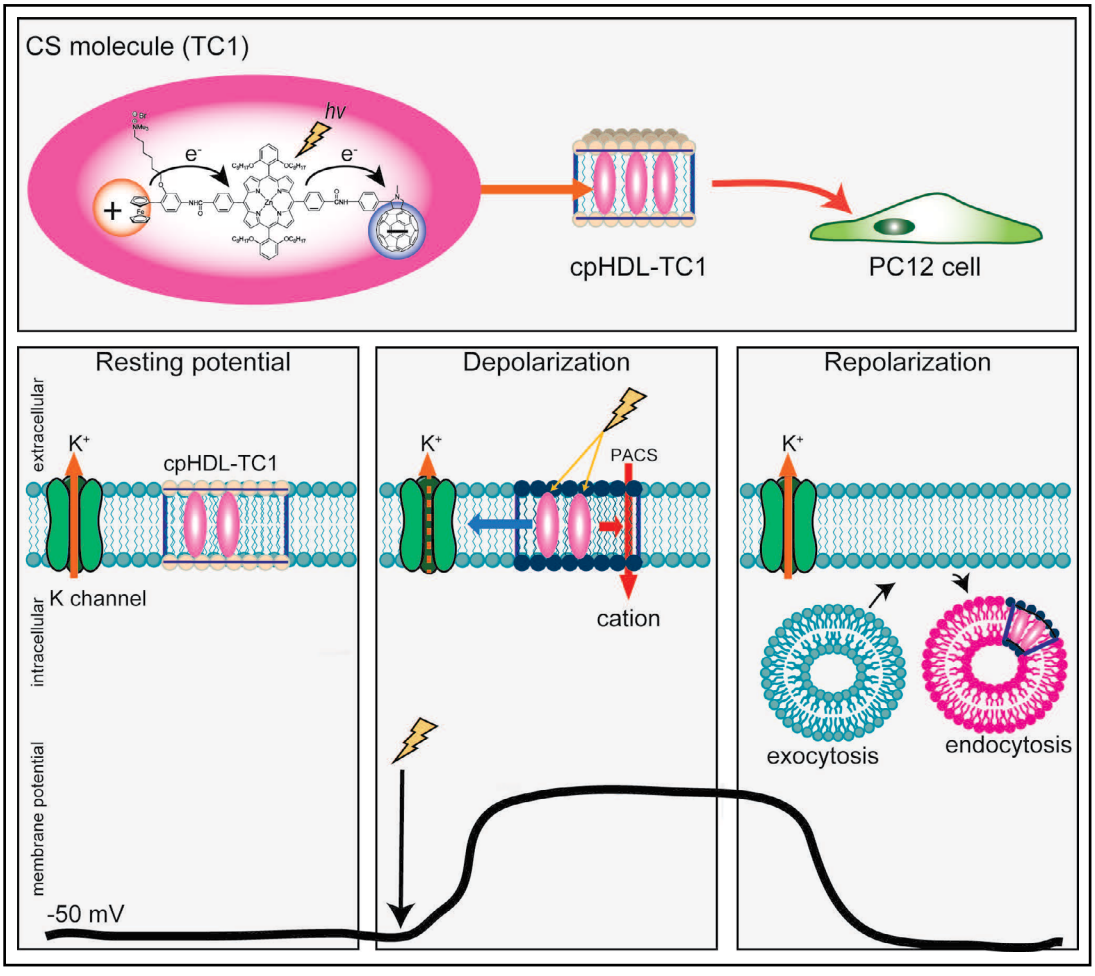

Fig. 8. Molecular mechanism of photo-induced depolarization with the initiation and repolarization of TC1. TC1 causes charge separation by photostimulation (hν). cpHDL-TC1 is generated by inserting TC1 into cpHDL and is properly introduced into the cell membrane of PC12 cells before measurement. The resting membrane potential shows a membrane potential of -50 mV due to the activity of the K channel. There is no change in resting membrane potential even in cells with cpHDL-TC1 inserted. Subsequently, Photo-activated TC1 causes depolarization by generating PACS (photo-activated CS molecule induced) current in parallel with the suppression of the K^+ current via the effect on lipid component (dark blue). This depolarization persists for a time, but the internalization of TC1 from the membrane and insertion of new lipids into the cell membrane, resulting in the restoration of K_v to normal activity and eliminating PACS currents, take place slowly.

cidated for depolarization and its reversibility. The rate of change in the light-induced membrane potential and membrane current was measured directly by the patch-clamp method in both the neural cell line and overexpression cell system treated with TC1. These depolarizing currents are basically irreversible, but exhibit reversibility in the form of repolarization upon membrane recycling. Here, for the first time, we demonstrate that the mechanism of light-induced depolarization of TC1 results from K_V channel activity suppression related to the resting membrane potential (Fig. 5) and the occurrence of PACS current with the loss of cell membrane capacitance (Fig. 2, 3). In addition, direct real-time recording of the current revealed that repolarization from depolarization was caused by TC1 internalization through endocytosis, and insertion of new membrane material through exocytosis (Fig. 6, 7). Notably, the membrane disk-shaped nanocarrier cpHDL enabled efficient light-induced depolarization by localizing the triad to the outer surface of the intact cell membrane (Fig. 1, 7). These results revealed a mechanism by which the light-induced TC1 activity, localized precisely at the cell membrane, caused a decrease in the plasma membrane resistance and subsequently sustained depolarization by K_V suppression and generation of PACS current. In addition, the intact cells restored K_V and PACS current through membrane recycling and achieved repolarization. We have previously observed that CS molecules, which do not have the same reactive oxygen species and cytotoxicity as TC1, have neural firing after photo-induced depolarization in cultured rat hippocampal neurons [26]. These findings suggest that the application of TC1 in combination with cpHDL can be used more efficiently and safely in biological applications.

Biological membranes play multiple physiological roles, such as physical barriers for ions and solutes, regulators of membrane protein function, and mediators of signal transduction. In particular, ion channel activity is moderately affected by substances that directly and indirectly affect cell membrane-protein interactions (polyunsaturated fatty acids such as arachidonic acid and DHA), and amphiphiles such as Triton X and capsaicin [27, 28]. Our results indicate that the endogenous and exogenous expression of voltage-gated K^+ channel activity is completely abolished, regardless of the molecular species. Thus, TC1 does not bind directly to the channel and is unlikely to stimulate specific membrane signaling. Indeed, the results in Fig. 6b, 6d, and 6e show that the K^+ channel function was not impaired for ~1 hour after 4 min of TC1 stimulation. However, the K^+ channel activity was restored indirectly by regeneration of cell membranes using the cytosis pathway. This is consistent with previous reports that such membrane lipids may affect the K^+ channel activity [29, 30]. Our results showed that voltage-dependent modulation of K^+ channel activity was not modulated, but was inactivated because it did not respond to voltage pulses after light-induced TC1 activation. Thus, the observations seen in the ion channel inactivation from the lipid quality changes are consistent with those of the gramicidin channel inactivation caused by oxide damage [31]. Our results showed that TC1 had no effect on membrane pore formation and recycling mechanism (Fig. 7), but had a significant effect on ion transport mechanism. An investigation of the properly tuned control of ion channel activity requires further study of the interaction between membrane lipids and ion channels.

Previous research on cell control using light-induced nanomaterials overlooked the possibility of membrane current generation from changes in the membrane quality [3]. Therefore, we considered the possibility of PACS currents through the membrane.

The most probable cause of a decreased membrane resistance is the ion channel activity. However, our observations showed no effect from the broad cation and anion channel inhibitor application (Fig. 3a–d), so the PACS current is unlikely to be the current through the ion channel. Second, CS molecules have been reported to generate very large voltages (~10^6 V/cm; 500 mV/5 nm) upon photostimulation [32]. Extremely high voltages on the membrane can reduce membrane resistance by forming pores in the membrane, as seen in electroporation technology [33]. Our results, as shown in Fig. 7c and 7d, show that very small molecules such as LDH (MW: 144 kDa) and PI (MW: 668.4 g/mol) do not pass through the membrane after TC1 stimulation (Fig. 7c and 7d). Thus, TC1 activity is unlikely to cause physical damage. Furthermore, TC1 has not been detected to generate reactive oxygen spe-

cies [12], and is therefore unlikely to be PACS current from membrane damage. Third, the possibility of changing the cell membrane properties can be understood by applying the idea of a dielectric breakdown, which is the basis of physics. The leakage current magnitude of a capacitor that has caused a dielectric breakdown is proportional to the damaged membrane capacitance (i.e., $I_{leak} \infty C_d = \varepsilon / t_d$; I_{leak}, leakage current; C_d, damaged capacitance; ε, dielectric constant; t_d, damaged membrane thickness). In our results, a 24.7% capacity loss was observed from the TC1 activity induced by photostimulation, which may be accompanied by PACS current (Fig. 3e). As described above, because the TC1 activity does not damage the cells, it is plausible that the PACS current occurs when the relative dielectric constant increases. Indeed, the dielectric constant of the damage was around 2 [34], but the previously reported dielectric constant of CS molecules of the same type as TC1 was ~4 in amphiphilic solvents [26]. Therefore, it is likely that TC1 activated in the cell membrane increased the cell membrane dielectric constant and lowered the membrane resistance.

Recently, an interdisciplinary study of physics and biology by Bezanilla and colleagues elucidated the mechanism by which a local temperature rise with near-infrared lasers caused instantaneous changes in the capacitance and leakage current [35]. The most recently, a research group by Lanzani and Benfenati has developed a method in which millisecond pulses of visible light induce transient hyperpolarization followed by a delayed depolarization that triggers action potential firing in neurons [36]. The administration of a photosensitive azobenzene compound to cells can be stimulated for 7 days without directly affecting the ion channels and local temperature. Although Near-infrared treatment and light-sensitive azobenzene treatment are very effective when applied to short-term neuronal cell excitement, our technique is that 5 minutes light irradiation of TC1-cpHDL can maintain cell excitement for 1 hour. It also has the advantage with regard to phototoxicity owing to drug metabolism. On the contrary, it is not suitable for treatment limited to short-term nerve stimulation. Therefore, it has potential medical applications in the regulation of autonomic excitability and endocrine cell secretion controlled by persistent excitability [37-40]. It is also important to note that the differentiating targets that can be stimulated in a cell-specific manner by improving cpHDL drug delivery system are candidates for advanced alternative tissue excitation techniques.

The integrity of cell membranes and membrane proteins depends on the endocytic and exocytotic pathways [41]. Although the membrane transport mechanisms of ion channels (including K^+ channels) have been demonstrated mainly through imaging and biochemical techniques, the direct real-time evaluation was inadequate [42]. Our results show that the assessment of ion channel activity during membrane recycling can be directly performed electrophysiologically in one hour in real time, which is the first study of this kind to our knowledge. Our CS-cpHDL also caused changes in membrane function on the target cells with light-induced timing. Therefore, the use of TC1 can be expected as a response tool for membrane research, such as autophagy and interaction analysis between membrane transport proteins and lipids.

Because the use of cpHDL improved the degree and rate of depolarization, improved cpHDL will certainly result in greater efficiency. Therefore, the use of recently developed cpHDL [43] that can achieve the efficient and appropriate targeted transport of CS molecules (such as cell membrane delivery efficiency) may contribute to the development of more efficient light-induced depolarization systems. For example, the absorption spectrum of TC1 solubilized with liposomes was reported to be similar to that in H_2O containing 10% DMSO, and their extinction coefficient at the excitation wavelength was also comparable [12]. Under this condition, the charge-separation quantum yield was decreased by >50% in the presence of liposomes, which could be accounted for by intermolecular electron transfer and self-quenching caused by unfavorable aggregation. In the same report, the number of TC1 molecules per cell was determined to be 1.9×10^6 upon its direct addition to cell culture media, which was one-tenth of $2–3 \times 10^7$ molecules/cell for the delivery by cpHDL [13]. In order to improve the charge separation yield, bioapplicable TC1s need to be improved by strategies that solve the problems of intermolecular aggregation and number of molecules in the cell membrane.

Experiments investigating the effect of TC1 on current with a voltage-clamp showed that most K^+ currents were suppressed during illumination of TC1-treated cells (Fig. 2). However, these results were lower than the expected K^+ channel-dependent depolarization values in response to the same TC1 treatment in current-clamp mode (Fig. 1). This value of depolarization suggests the involvement of Na^+-K^+ pumps [44] and Cl^- channels [45, 46] that form the resting membrane potential, and the effects of TC1 on the activity of these targets require further study.

Further research is needed to better characterize the depolarization and repolarization mechanisms of TC1 photostimulation, and to explore how that knowledge could enhance the use of this technology *in vivo*. For example, it would be interesting to model the effect of TC1 on intramolecular lipid dipole moments at the molecular level and the interaction of lipids experienced by voltage-gated K^+ channels. It may also help to understand the membrane properties of various cell types expressed *in vivo* and analyze whether they mediate downstream physiological effects. Herein, we demonstrated that TC1 photostimulation affects the membrane potential via ion transport by altering cell membrane properties, including cell membrane resistance. Our discovery supports the application of this unique optical technology as a tool in physics, biology, pharmacology and medicine.

Conclusion

The ability to non-invasively alter cell membrane excitability, via unique light-controlled depolarization applications, has attractive therapeutic translation potential. The light-induced regulation of membrane potentials with drug delivery systems is fascinating as a strategy for promoting research on the biological processes of excitable cells, and for the spatiotemporal control of the nervous system and muscle activity. Our findings concluded that depolarization of the CS molecule simultaneously inactivates the voltage-dependent potassium currents and produces PACS currents. This activity continues to depolarize target cells, but is reversible via a regeneration mechanism because the cell membrane is intact. Unraveling the underlying mechanism of cellular photoexcitation highlights the generality of membrane excitability regulation and potential medical applications to autonomic nerves and secretory organ that exert physiological function by continuous excitation.

Acknowledgements

We thank Mr. Masahiro Ohara (National Institute for Physiological Science) for helpful discussion. We thank Rosalie Tran, PhD, from Edanz Group (https://en-author-services.edanzgroup.com/) for editing a draft of this manuscript.

Author contributions

T.N. conducted all experiments and analysis. R.F. and T.M. conducted the CS molecule and drug delivery system experiments. H.M. and Y.K. performed the PCR experiments. K.S-N. assisted in the culture design, imaging analysis, and discussion of the data. H.I. and T.M. discussed and commented on the draft. T.N. conceived and designed the work, and wrote the manuscript.

Funding Sources

This work was supported in part by Grants in-Aid for Scientific Research (KAKENHI) from the Japan Society for the Promotion of Science and the Ministry of Education, Culture, Sports, Science (No. 15K08197 and 18K06864), and Central Research Institute of Fukuoka University (No. 177009).

Disclosure Statement

The authors have no conflicts of interest to declare.

References

1 Ordaz J, Wu W, Xu XM: Optogenetics and its application in neural degeneration and regeneration. Neural Regen Res 2017;12:1197-1209.
2 Szobota S, Isacoff EY: Optical control of neuronal activity. Annu Rev Biophys 2010;39:329-348.
3 Wang Y, Guo L: Nanomaterial-Enabled Neural Stimulation. Front Neurosci 2016;10:69.
4 Thang DC, Wang Z, Lu X, Xing B: Precise cell behaviors manipulation through light-responsive nano-regulators: recent advance and perspective. Theranostics 2019;9:3308-3340.
5 Ellis-Davies GCR: Useful Caged Compounds for Cell Physiology. Acc Chem Res 2020;53:1593-1604.
6 Ellis-Davies GC: Caged compounds: photorelease technology for control of cellular chemistry and physiology. Nat Methods 2007;4:619-628.
7 Ankenbruck N, Courtney T, Naro Y, Deiters A: Optochemical Control of Biological Processes in Cells and Animals. Angew Chem Int Ed Engl 2018;57:2768-2798.
8 Yin S, Liu J, Kang Y, Lin Y, Li D, Shao L: Interactions of nanomaterials with ion channels and related mechanisms. Br J Pharmacol 2019;176:3754-3774.
9 Hüll K, Morstein J, Trauner D: In Vivo Photopharmacology. Chem Rev 2018;118:10710-10747.
10 Paoletti P, Ellis-Davies GCR, Mourot A: Optical control of neuronal ion channels and receptors. Nat Rev Neurosci 2019;20:514-532.
11 Hoorens MWH, Szymanski W: Reversible, Spatial and Temporal Control over Protein Activity Using Light. Trends Biochem Sci 2018;43:567-575.
12 Cai N, Takano Y, Numata T, Inoue R, Mori Y, Murakami T, Imahori H: Strategy to Attain Remarkably High Photoinduced Charge-Separation Yield of Donor–Acceptor Linked Molecules in Biological Environment via Modulating Their Cationic Moieties. J Phys Chem C 2017;121:17457-17465.
13 Numata T, Murakami T, Kawashima F, Morone N, Heuser JE, Takano Y, Ohkubo K, Fukuzumi S, Mori Y, Imahori H: Utilization of photoinduced charge-separated state of donor-acceptor-linked molecules for regulation of cell membrane potential and ion transport. J Am Chem Soc 2012;134:6092-6095.
14 Murakami T, Wijagkanalan W, Hashida M, Tsuchida K: Intracellular drug delivery by genetically engineered high-density lipoprotein nanoparticles. Nanomedicine 2010;5:867-879.
15 Suda K, Murakami T, Gotoh N, Fukuda R, Hashida Y, Hashida M, Tsujikawa A, Yoshimura N: High-density lipoprotein mutant eye drops for the treatment of posterior eye diseases. J Control Release 2017;266:301-309.
16 Rae J, Cooper K, Gates P, Watsky M: Low access resistance perforated patch recordings using amphotericin B. J Neurosci Methods 1991;37:15-26.
17 Neher E, Marty A: Discrete changes of cell membrane capacitance observed under conditions of enhanced secretion in bovine adrenal chromaffin cells. Proc Natl Acad Sci U S A 1982;79:6712-6716.
18 Horn R, Marty A: Muscarinic activation of ionic currents measured by a new whole-cell recording method. J Gen Physiol 1988;92:145-159.
19 Leech CA, Holz GGt: Application of patch clamp methods to the study of calcium currents and calcium channels. Methods Cell Biol 1994;40:135-151.
20 Wang X, Cao Y, Shen M, Wang B, Zhang W, Liu Y, He X, Wang L, Xia Y, Ding M, Xu X, Ren J: DIDS Reduces Ischemia/Reperfusion-Induced Myocardial Injury in Rats. Cell Physiol Biochem 2015;35:676-688.
21 Peña F, Ordaz B: Non-selective cation channel blockers: potential use in nervous system basic research and therapeutics. Mini Rev Med Chem 2008;8:812-819.
22 Conforti L, Millhorn DE: Selective inhibition of a slow-inactivating voltage-dependent K+ channel in rat PC12 cells by hypoxia. J Physiol 1997;502:293-305.
23 Johnston J, Forsythe ID, Kopp-Scheinpflug C: Going native: voltage-gated potassium channels controlling neuronal excitability. J Physiol 2010;588:3187-3200.

24 Zaczek R, Chorvat RJ, Saye JA, Pierdomenico ME, Maciag CM, Logue AR, Fisher BN, Rominger DH, Earl RA: Two new potent neurotransmitter release enhancers, 10,10-bis(4-pyridinylmethyl)-9(10H)-anthracenone and 10,10-bis(2-fluoro-4-pyridinylmethyl)-9(10H)-anthracenone: comparison to linopirdine. J Pharmacol Exp Ther 1998;285:724-730.
25 Idone V, Tam C, Andrews NW: Two-way traffic on the road to plasma membrane repair. Trends Cell Biol 2008;18:552-559.
26 Takano Y, Numata T, Fujishima K, Miyake K, Nakao K, Grove WD, Inoue R, Kengaku M, Sakaki S, Mori Y, Murakami T, Imahori H: Optical control of neuronal firing via photoinduced electron transfer in donor-acceptor conjugates. Chem Sci 2016;7:3331-3337.
27 Cordero-Morales JF, Vásquez V: How lipids contribute to ion channel function, a fat perspective on direct and indirect interactions. Curr Opin Struct Biol 2018;51:92-98.
28 Lundbaek JA: Lipid bilayer-mediated regulation of ion channel function by amphiphilic drugs. J Gen Physiol 2008;131:421-429.
29 Dart C: SYMPOSIUM REVIEW: Lipid microdomains and the regulation of ion channel function. J Physiol 2010;588:3169-3178.
30 Hite RK, Butterwick JA, MacKinnon R: Phosphatidic acid modulation of Kv channel voltage sensor function. eLife 2014;3:e04366.
31 Stark G: Functional Consequences of Oxidative Membrane Damage. J Membr Biol 2005;205:1-16.
32 Gosztola D, Yamada H, Wasielewski MR: Electric Field Effects of Photogenerated Ion Pairs on Nearby Molecules: A Model for the Carotenoid Band Shift in Photosynthesis. J Am Chem Soc 1995;117:2041-2048.
33 Aycock KN, Davalos RV: Irreversible Electroporation: Background, Theory, and Review of Recent Developments in Clinical Oncology. Bioelectricity 2019;1:214-234.
34 Huang W, Levitt DG: Theoretical calculation of the dielectric constant of a bilayer membrane. Biophys J 1977;17:111-128.
35 Shapiro MG, Homma K, Villarreal S, Richter CP, Bezanilla F: Infrared light excites cells by changing their electrical capacitance. Nat Commun 2012;3:736.
36 DiFrancesco ML, Lodola F, Colombo E, Maragliano L, Bramini M, Paternò GM, Baldelli P, Serra MD, Lunelli L, Marchioretto M, Grasselli G, Cimò S, Colella L, Fazzi D, Ortica F, Vurro V, Eleftheriou CG, Shmal D, Maya-Vetencourt JF, Bertarelli C, Lanzani G, et al: Neuronal firing modulation by a membrane-targeted photoswitch. Nat Nanotechnol 2020;15:296-306.
37 Fletcher PA, Sherman A, Stojilkovic SS: Common and diverse elements of ion channels and receptors underlying electrical activity in endocrine pituitary cells. Mol Cell Endocrinol 2018;463:23-36.
38 Toescu EC, Dayanithi G: Neuroendocrine signalling: natural variations on a Ca2+ theme. Cell Calcium 2012;51:207-211.
39 Ozawa S, Sand O: Electrophysiology of excitable endocrine cells. Physiol Rev 1986;66:887-952.
40 Williams JA: Electrical correlates of secretion in endocrine and exocrine cells. Fed Proc 1981;40:128-134.
41 Balse E, Boycott HE: Ion Channel Trafficking: Control of Ion Channel Density as a Target for Arrhythmias? Front Physiol 2017;8:808-808.
42 Steele DF, Eldstrom J, Fedida D: Mechanisms of cardiac potassium channel trafficking. J Physiol 2007;582:17-26.
43 Kim H, Nobeyama T, Honda S, Yasuda K, Morone N, Murakami T: Membrane fusogenic high-density lipoprotein nanoparticles. Biochim Biophys Acta Biomembr 2019;1861:183008.
44 Pivovarov AS, Calahorro F, Walker RJ: Na(+)/K(+)-pump and neurotransmitter membrane receptors. Invert Neurosci 2018;19:1.
45 Funabashi K, Fujii M, Yamamura H, Ohya S, Imaizumi Y: Contribution of Chloride Channel Conductance to the Regulation of Resting Membrane Potential in Chondrocytes. J Pharmacol Sci 2010;113:94-99.
46 Blatz AL, Magleby KL: Single chloride-selective channels active at resting membrane potentials in cultured rat skeletal muscle. Biophys J 1985;47:119-123.